INTERNATIONAL JOURNAL FOR NUMERICAL METHODS IN ENGINEERING

Int. J. Numer. Meth. Engng 2014; **00**:1–36

Published online in Wiley InterScience (www.interscience.wiley.com). DOI: 10.1002/nme

An adaptive spectral Galerkin stochastic finite element method using variability response functions

Dimitris G. Giovanis*,Vissarion Papadopoulos,George Stavroulakis

Institute of Structural Analysis and AntiSeismic Research, National Technical University of Athens, Iroon Polytechniou 9, Zografou Campus, Athens 15780, Greece

SUMMARY

A methodology is proposed in this paper to construct an adaptive sparse polynomial chaos (PC) expansion of the response of stochastic systems whose input parameters are independent random variables modeled as random fields. The proposed methodology utilizes the concept of variability response function (VRF) in order to compute an a priori low cost estimate of the spatial distribution of the second-order error of the response, as a function of the number of terms used in the truncated Karhunen-Lo eve (KL) expansion. This way the influence of the response variance to the spectral content (correlation structure) of the random input is taken into account through a spatial variation of the truncated KL terms. The criterion for selecting the number of KL terms at different parts of the structure is the uniformity of the spatial distribution of the second order error. This way a significantly reduced number of PC coefficients, with respect to classical PC expansion, is required in order to reach a uniformly distributed target second-order error. This results in an increase of sparsity of the coefficient matrix of the corresponding linear system of equations leading to an enhancement of the computational efficiency of the spectral stochastic finite element method (SSFEM).

Received . . .

KEY WORDS: Spectral stochastic finite element analysis, Variability response function, Polynomial chaos, Karhunen-Loève decomposition, adaptivity

*Correspondence to: dgiov16@yahoo.gr

1. INTRODUCTION

It is common knowledge that the analysis of structural systems with ambiguous characteristics has been the focal point of research work over the course of the last two decades. Epistemic uncertainty can be taken into consideration in simulation by setting the problem in a probabilistic framework, resulting in governing equations that are, in general, stochastic partial differential equations. Throughout this period of time, a plethora of stochastic finite element methodologies (SFEM) for the numerical solution of the aforementioned stochastic partial differential equations have been developed [1]. Especially, the application of the Polynomial Chaos (PC) expansion within the SFEM has drawn significant attention with the introduction of the so-called Spectral SFEM (SSFEM) [2], where the Karhunen-Loève (KL) [3] representation is employed to model the uncertain input parameters, while the stochastic responses are propagated using the PC formulation based on Galerkin minimization scheme as well as the application of the polynomial dimensional decomposition (PDD) [4, 5] method which is based on a hierarchical decomposition of a multivariate response function in terms of variables with increasing dimensions. A comparison of the PCE and PDD approximations can be found in [6] where it is shown that significant differences in terms of accuracy, efficiency, and convergence properties exist between the two approaches due to their truncation. For both the PCE and PDD expansions the independent assumption is commonly adopted by most researchers. However, in reality, there may exist significant correlation or dependence among input variables. In this case commonly used transformation methods (e.g Rosenblatt) usually degrade the convergence properties of probabilistic solutions. A recent work [7] addresses dependent variables head on and explicitly, that is, without invoking any transformations.

It could be argued that one of the most blurry areas of the PCE-based methods, where the system response is underpinned by a set of polynomials of the fundamental random variables, is the computational effort involved, especially in cases where the corresponding random input is described by a non-Gaussian marginal distribution and the truncation order of the KL as well as of the PC order are high. In these cases, the sparsity of the corresponding deterministic matrix that has to be inverted is decreased, leading in a dramatic increase of the required computational

Prepared using nmeauth.cls DOI: 10.1002/nme

effort. Stochastic adaptivity and model reduction techniques for the SSFEM have been proposed in [8, 9, 10] in an effort to reduce the overall problem dimensionality and augment the sparsity of the deterministic matrix, in tandem with efficient preconditioning and domain decomposition-based approaches which reduce the computational cost encountered in the inversion of coupled deterministic problems [11, 12]. Regarding the PDD method, an adaptive variant was recently introduced in [13] where global sensitivity indices are used to truncate the PDD.

The concept of variability response function (VRF) was introduced by Shinozuka in the late 1980s [14] in order to provide information of the spatial distribution of the variability of a structure's response with no information of the spatial correlation structure of the uncertain system parameters. The VRF is a deterministic function dependent on the structure, its boundary conditions and loading, assumed to be independent of the distributional and spectral characteristics of the uncertain system parameters. It identifies the sensitivity of the correlation structure of the uncertain parameters on the variability of the response. Although VRFs were initially proposed for relatively simple statically determinant structures, subsequent developments allowed for their successful implementation to general stochastic finite element while recent advances include extention of this approach to non-linear problems [15]. Different aspects and applications of the VRF were introduced in [16, 17, 18, 19, 20, 21], while an efficient fast Monte Carlo simulation for the numerical computation of VRF of this approach was provided in [16, 22]. A development of this approach, which further boosted the validity of the assumption of independence of VRF to the stochastic parameters of the problem, was proposed in [23] where the concept of generalized VRF (GVRF) was introduced which is derived from a family of different VRFs for corresponding combinations of different pdfs with different sets of power spectral density functions.

Summarizing, PC expansions are used in the framework of SFEM to represent the uncertain parameters as well as the response of the system by a set of coefficients in a suitable random polynomial basis. The implementation of classical solution schemes (i.e. Galerkin) for the estimation of the PC coefficients leads to a system of coupled deterministic equations. However, solving this coupled system becomes unaffordable, especially if the number of terms in the truncated

Prepared using nmeauth.cls
DOI: 10.1002/nme

KL as well as the order of the PC are high and/or a PC expansion is also used for the descritization of the random input (i.e non-Gaussian correlation structures). Motivated by this drawback of the SSFEM method the present paper describes a methodology in which the concept of VRF is utilized for an a priori low-cost estimate of the spatial distribution of the statistical second-order error of the response, as a function of the truncation order of the KL decomposition. This is how the sensitivity of the response variance towards the spectral content (correlation structure) of the random input is taken into consideration by means of a spatial variation of the truncated KL terms. The basic criterion for the selection of the number of KL terms at different locations of the structure is in essence the uniformity displayed of the spatial distribution of the second order error. This way a significantly decreased amount of PC coefficients, with regard to classical PC expansion, is required in order to reach a uniformly distributed target second-order error. This variation of the KL terms leads to a certain increase of sparsity of the coefficient matrix of the corresponding augmented linear system of equations, thus resulting into the embellishment of the computational efficiency of the SSFEM. This enhancement of the computational efficiency is demonstrated with a comparison between the computing time required for the solution of the full SSFEM formulation and the corresponding sparse one. In both cases a standard Preconditioner Conjugate Gradient (PCG) iterative method with a block-diagonal preconditioner was implemented as a reference solution scheme for the assessment of the computational performance of the proposed methodology [24, 25].

The remainder of this paper is organized as follows. In Section 2, the theoretical background of modeling Gaussian and non-Gaussian random fields using the KL and PC expansions, respectively, is described. Section 3 contains a brief description of the SSFEM. Section 5 describes a solution method for the stochastic partial differential equations. The proposed method is overviewed in Section 6 while Section 7 reports performance results in an attempt to demonstrate both the effectiveness and the applicability of the proposed methodology. Last but not least, in Section 8 numerical data is presented demonstrating the computational merits of the proposed methodology in terms of the computational performance.

Prepared using nmeauth.cls
DOI: 10.1002/nme

2. MODELING OF UNCERTAIN STRUCTURAL PARAMETERS

2.1. Gaussian random fields

In terms of discretization error, an efficient decomposition of a zero-mean Gaussian random field is the Karhunen-Loève (KL) expansion [3, 26, 27] which approximates it by a linear combination of orthogonal deterministic functions with independent standard Gaussian random variables, where the orthogonal deterministic functions and their magnitude are the eigenfunctions and eigenvalues of the covariance function, respectively. The KL expansion of a multi-dimensional random field $f(\mathbf{x}, \theta)$ is written as:

$$f(\mathbf{x}, \theta) = \mu(\mathbf{x}) + \sum_{i=1}^{\infty} \sqrt{\lambda_i} \xi_i(\theta) \phi_i(\mathbf{x}) \tag{1}$$

$\mathbf{x} \in \mathbb{R}^n,\ n = 1, 2, 3$ being a position variable and θ the random event. In eq.(1) $\mu(\mathbf{x})$ is the mean value of the random field, λ_i and $\phi_i(\mathbf{x})$ are the eigenvalues and eigenfunctions of its covariance function $C(\mathbf{x}_1, \mathbf{x}_2)$. By definition, $C(\mathbf{x}_1, \mathbf{x}_2)$ is bounded, symmetric and positive definite with the following spectral or eigen-decomposition:

$$C(\mathbf{x}_1, \mathbf{x}_2) = \sum_{i=1}^{\infty} \lambda_i \phi_i(\mathbf{x}_1) \phi_i(\mathbf{x}_2) \tag{2}$$

The eigenvalues and eigenfunctions of $C(\mathbf{x}_1, \mathbf{x}_2)$ may be calculated, in the range D of the random process $f(\mathbf{x}, \theta)$, from the solution of the homogeneous Fredholm integral equation of the second kind given by:

$$\int_D C(\mathbf{x}_1, \mathbf{x}_2) \phi_i(\phi_1) = \lambda_i \phi_i(\phi_2) \tag{3}$$

The parameter $\xi_i(\theta)$ in eq.(1) is a set of uncorrelated Gaussian random variables which can be expressed as

$$\xi_i(\theta) = \frac{1}{\sqrt{\lambda_i}} \int_D [f(\mathbf{x}, \theta) - \mu(\mathbf{x})] \phi_i(\mathbf{x}) d\mathbf{x} \tag{4}$$

with mean and covariance function given by:

$$\begin{aligned} E[\xi_i(\theta)] &= 0 \\ E[\xi_i(\theta) \xi_j(\theta)] &= \delta_{ij} \end{aligned} \tag{5}$$

For practical purposes, the KL series expansion of eq.(1) is approximated by a finite number of M

Prepared using nmeauth.cls
DOI: 10.1002/nme

terms, giving

$$f(\mathbf{x},\theta) \simeq \widehat{f}(\mathbf{x},\theta) = \mu(\mathbf{x}) + \sum_{i=1}^{M} \sqrt{\lambda}_i \xi_i(\theta)\phi_i(\mathbf{x}) \tag{6}$$

and corresponding covariance function

$$\widehat{C}(\mathbf{x}_1,\mathbf{x}_2) = \sum_{i=0}^{M+1} \lambda_i \phi_i(\mathbf{x}_1)\phi_i(\mathbf{x}_2) \tag{7}$$

2.2. Non-Gaussian random fields

However, the Gaussian fields are not well suited to modeling material properties (Young's modulus, yield stress, etc.) which are by their nature positive valued. Indeed, when a large dispersion of the parameter is considered, choosing a Gaussian representation can easily lead to negative realizations of the parameter, which have no physical meaning (in contrast, the lognormal field appears attractive in this sense). On the other hand, if the parameter under consideration is modeled by a non-Gaussian random field, it is not possible to expand it as a linear expression in standard normal variable space as in Eq. (6). In this case, non-Gaussian random fields $g(\mathbf{x})$ can be obtained by translation field theory [28, 29] which combines mathematical rigorousness and wide applicability in engineering and applied science. It provides a framework for simulation of processes and fields according to a prescribed Autocorrelation Function (ACF) or equivalently Power Spectral Density Function (PSDF) and a marginal non-Gaussian Probability Density Function (PDF). A descritized non-Gaussian field $\widehat{g}(\mathbf{x})$ can be obtained by a Gaussian random field $\widehat{h}(\mathbf{x})$ using a nonlinear transformation $h(\cdot)$:

$$\widehat{g}(\mathbf{x}) = h(\widehat{f}(\mathbf{x})) \tag{8}$$

Other techniques have also been developed for simulation of non-Gaussian stochastic fields. One important group of such techniques are those utilizing KL expansion and PC expansion such as those by Sakamoto and Ghanem [30, 31]. In order to be able to include lognormal fields in the SSFEM approach, Ghanem [32] proposed to expand them into the PC basis as

$$\widehat{g}(\mathbf{x}) = e^{(\widehat{f}(\mathbf{x}))} = \sum_{i=0}^{P} y_i \cdot \Psi_i \tag{9}$$

Prepared using nmeauth.cls
DOI: 10.1002/nme

where Ψ_i is constructed from Hermite polynomials. According to the classic truncation scheme [2, 33] the number of coefficients in the PC is given by

$$P = \frac{(M+p)!}{M!p!} \tag{10}$$

In view of the orthogonality of the Ψ_i variables,

$$\begin{aligned} \langle \Psi_i \rangle &= 0 \\ \langle \Psi_i \Psi_j \rangle &= \langle \Psi_i^2 \rangle \delta_{ij} \end{aligned} \tag{11}$$

where δ_{ij} is the Kronecker-delta function, the coefficients y_i can be obtained as

$$y_i = \frac{\langle \Psi_i \cdot e^f \rangle}{\langle \Psi_i^2 \rangle} \tag{12}$$

Although for any arbitrary random field with finite second-order moments the Hermite-chaos expansion converges efficiently [34], it has been demonstrated that the convergence rate is optimal for Gaussian fields; in fact the rate is exponential [35]. This can be understood from the fact that the weighting function of Hermite polynomials is the same as the probability density function of the Gaussian random variables. For non-Gaussian random fields the convergence rate may be substantially slower. In this case, other types of orthogonal polynomials, instead of Hermite polynomials, could use to construct the chaos expansion such as measure-consistent polynomials which be obtained analytically for lognormal random fields [5].

The numerator of eq.(12) can be rewritten as

$$\langle \Psi_i \cdot e^f \rangle = \int_{-\infty}^{+\infty} \Psi(\boldsymbol{\xi}) \exp[g - \frac{1}{2}\boldsymbol{\xi}^T \boldsymbol{\xi}] \tag{13}$$

This integral can be evaluated in closed form resulting in

$$y_i = \frac{\langle \Psi(\boldsymbol{\eta}) \rangle}{\langle \Psi_i^2 \rangle} \exp[\mu_g + \frac{1}{2}\sum_{i=0}^{P} g_i] \tag{14}$$

where $\Psi(\boldsymbol{\eta})$ can be found in [32].

Prepared using nmeauth.cls
DOI: 10.1002/nme

3. USING GALERKIN-BASED PC EXPANSION FOR THE PROPAGATION OF STRUCTURAL RESPONSES

Aside from the modeling of random input parameters, the PC formulation so far has been mostly used in order to propagate the stochastic responses. In the Galerkin based approach, the deterministic PC coefficients are calculated by solving the system of linear equations derived by forcing the residual to be orthogonal to the approximation space. Consider a stochastic finite element system with deterministic boundary conditions, deterministic loading and a stochastic system property (i.e. modulus of elasticity). The equilibrium equations for the system can be written as follows:

$$\hat{\mathbf{K}}\hat{\mathbf{U}} = \mathbf{F} \tag{15}$$

where $\hat{\mathbf{K}}$ denotes the stochastic stiffness matrix, $\hat{\mathbf{U}}$ is the stochastic displacement vector and $\mathbf{F}$ stands for the deterministic force vector. The stochastic matrix can be approximated in the following form

$$\hat{\mathbf{K}} = \sum_{i=0}^{M+1} \mathbf{k}_i \xi_i \tag{16}$$

In the above equation, $\mathbf{k}_0$ stands for the mean stiffness matrix and $\mathbf{k}_i$ are deterministic matrices of size $N \times N$. Using the PC expansion in order to represent the stochastic displacement vector $\hat{\mathbf{U}}$ leads to,

$$\hat{\mathbf{U}} = \sum_{j=0}^{P-1} \mathbf{u}_j \Psi_j \tag{17}$$

where $\mathbf{u}_j$ are N dimensional vectors of deterministic coefficients to be calculated. Substituting the expressions for $\hat{\mathbf{K}}$ and $\hat{\mathbf{U}}$ into eq.(15) and adopting the Galerkin approach leads to the following system of linear equations,

$$\sum_{j=0}^{M+1} \sum_{i=0}^{P-1} c_{ijk} \mathbf{k}_i \mathbf{u}_j = \langle \mathbf{F} \Psi_k \rangle \tag{18}$$

where $c_{ijk} = \langle \xi_i \Psi_j \Psi_k \rangle$ is a deterministic quantity, which depends on the dimension and order of the expansion only. This system of equations can be expressed as

$$\mathcal{K} \cdot \mathcal{U} = \mathcal{F} \tag{19}$$

where,

Prepared using nmeauth.cls
DOI: 10.1002/nme

$$\mathcal{K} = \begin{bmatrix} \sum_{i=0}^{M+1} c_{i,0,0}\mathbf{k}_i & \sum_{i=0}^{M+1} c_{i,1,0}\mathbf{k}_i & \cdots & \sum_{i=0}^{M+1} c_{i,P,0}\mathbf{k}_i \\ \sum_{i=0}^{M+1} c_{i,0,1}\mathbf{k}_i & \sum_{i=0}^{M+1} c_{i,1,1}\mathbf{k}_i & \cdots & \sum_{i=0}^{M+1} c_{i,P,1}\mathbf{k}_i \\ \vdots & \vdots & \ddots & \vdots \\ \sum_{i=0}^{M+1} c_{i,0,P-1}\mathbf{k}_i & \sum_{i=0}^{M+1} c_{i,1,P-1}\mathbf{k}_i & \cdots & \sum_{i=0}^{M+1} c_{i,P-1,P-1}\mathbf{k}_i \end{bmatrix}$$

$$\mathcal{U} = \begin{bmatrix} \mathbf{u}_0, & \mathbf{u}_1, & \cdots, & \mathbf{u}_{P-1} \end{bmatrix}^T$$

$$\mathcal{F} = \begin{bmatrix} \mathbf{F}_0, & \mathbf{F}_1, & \cdots, & \mathbf{F}_{P-1} \end{bmatrix}^T$$

After solving the system we obtain the coefficients $\mathbf{u}_j$ and we can estimate the displacement vector from eq.(17).If the random field is lognormal the stiffness matrix $\hat{\mathbf{K}}$ can be approximated using the PC expansion,

$$\hat{\mathbf{K}} = \sum_{i=0}^{P-1} \mathbf{k}_i \Psi_i \tag{20}$$

leading to

$$\sum_{j=0}^{P-1} \sum_{i=0}^{P-1} d_{ijk}\mathbf{k}_i\mathbf{u}_j = \langle \mathbf{F}\Psi_k \rangle \tag{21}$$

where $d_{ijk} = \langle \Psi_i \Psi_j \Psi_k \rangle$. In this case however, the solution of the system is computationally more demanding because d_{ijk} contains more non-zero elements compared to c_{ijk}. Once the coefficients of the expansion are computed, approximate statistics of the solution can be derived by Monte Carlo simulation (MCS). In this case however, MCS is costless since it is applied directly to a polynomial representation without the need of solving a system of equations.

4. VARIABILITY RESPONSE FUNCTION

The variability response function (VRF) is a deterministic function that identifies the sensitivity of a response quantity to the correlation structure (or spectral contents), of a property of the structure that is modeled as a homogeneous random field. It has been demonstrated that the VRF depends only on deterministic parameters related to the geometry, material properties and loading of the structure, as well as on the standard deviation σ_f of the random parameter (for statically determinate structures, VRF is independent of σ_f as well [16]). The VRF's concept is defined as

Prepared using nmeauth.cls
DOI: 10.1002/nme

$$\mathrm{Var}[U_i] = \int_{-\infty}^{\infty} \mathrm{VRF}_i(\kappa, \sigma_f) \cdot S_f(\kappa) d\kappa \tag{22}$$

where $S_f(\kappa)$ is the power spectrum of the stochastic field defined over the wave number domain κ. From eq.(25) we can estimate the variance of the displacement field (in each degree of freedom i) of a linear SFEM under static loading. The major drawback of this method is that it can effectively provide with up to second order information of the stochastic system response. Thus, if higher order moments of the marginal pdf of the response is required, one must resort to a classical intrusive or non-intrusive approach.

4.1. Fast Monte Carlo simulation

The variability response function can be estimated numerically using a fast Monte Carlo simulation (FMCS) approach whose basic idea is to consider the stochastic field $f(x)$ as a random sinusoid. The numerical estimation of the VRF through FMCS is extremely important as the closed-form analytic expressions involve modulating functions that are very difficult to establish. For this reason, FMCS is used exclusively to determine the VRF. The basic steps of the FMCS approach are described in the following.

1 For every wave number $\overline{\kappa}$ generate N sample functions of the stochastic field $f(x)$ as a random sinusoid with standard deviation σ_f:

$$f_j(x) = \sqrt{2}\sigma_f \cos(\overline{\kappa}x + \phi_j) \quad j = 1, 2, ..., N \tag{23}$$

where ϕ_j are random phase angles uniformly distributed in the range $[0, 2\pi]$. Rather than picking up the ϕ_j s randomly in $[0, 2\pi]$, they can be selected at N equal intervals in $[0, 2\pi]$ for significant computational savings.

2 Using these N generated sample functions of $f_j(x)$, it is straightforward to compute the corresponding N displacement responses either analytically or numerically. Then, the mean value of the response $\varepsilon[U_i]_{\overline{\kappa}}$ and its variance $\mathrm{Var}[U_i]_{\overline{\kappa}}$ can be easily determined for the specific value of $\overline{\kappa}$ considered by ensemble averaging the N computed responses.

3 The value of the VRF_i at degree of freedom i, for wave number $\overline{\kappa}$ and for standard deviation σ_f is computed from

Prepared using nmeauth.cls
DOI: 10.1002/nme

$$\text{VRF}_i(\overline{\kappa}, \sigma_f) = \frac{\text{Var}[U_i]_{\overline{\kappa}}}{\sigma_f^2},\ i = 1, \ldots, n_{dof} \tag{24}$$

where n_{dof} is the total number of degrees of freedom.

4 Steps $1-3$ are repeated for different values of the wave number $\overline{\kappa}$ of the random sinusoid. Consequently $\text{VRF}_i(\overline{\kappa}, \sigma_f)$ are computed over a wide range of wave numbers, wave number by wave number. The entire procedure can be eventually repeated for different values of the standard deviation σ_f.

It should be pointed out that the FMCS can be implemented into the framework of a deterministic finite element code making this approach very general. For a two-dimensional random field VRF is defined as

$$\begin{aligned} \text{Var}[U_i] &= \int_{-\infty}^{\infty}\int_{-\infty}^{\infty} \text{VRF}_i(\kappa_1, \kappa_2) S_f(\kappa_1, \kappa_2) d\kappa_1 d\kappa_2 \\ &= 4(\Delta\kappa)^2 \sum_{i=1}^{n}\sum_{j=1}^{n} \text{VRF}_i(\kappa_i, \kappa_j) S_f(\kappa_i, \kappa_j) \end{aligned} \tag{25}$$

and eq.(23) is replaced by

$$f_j(x, y) = \sqrt{2}\sigma_f \cos(\kappa_1 x + \kappa_2 y + \phi_j) \quad j = 1, 2, ..., N \tag{26}$$

5. SOLUTION OF THE SYSTEM OF STOCHASTIC PARTIAL DIFFERENTIAL EQUATIONS

5.1. Monte Carlo methods

When dealing with deterministic external loading, the FMCS procedure of section 4.1 for the estimation of the mean value of the response in every wave number $\overline{\kappa}$ features the solution of successive linear systems with multiple left-hand sides, since only the coefficient matrix $\mathbf{K}$ changes in every simulation. Due to the fact that the solution process has to start from the beginning, a new stiffness matrix needs to be formed at each simulation. Such solution can be performed either with a standard direct method based on Cholesky factorization or with iterative methods.

In order to alleviate the incapability of direct schemes to exploit the proximity of the resulting systems of equations, iterative solvers have been proposed which are customized to the particular

Prepared using nmeauth.cls
DOI: 10.1002/nme

properties of the equilibrium equations arising in the context of MCS methods. The resulting near-by problems can be effectively solved using the preconditioned conjugate gradient (PCG) algorithm, equipped with a preconditioner following the rationale of incomplete Cholesky preconditioning [36, 37, 38]. This solution procedure consists of utilizing the deterministic $\mathbf{K}_0$ stiffness matrix as its preconditioner throughout the entire simulation process for the solution of the near-by problems.

The PCG algorithm, when solving a linear system of the form $\mathbf{Ax} = \mathbf{b}$ with a preconditioner $\tilde{\mathbf{A}}$, is depicted in Table 1 for iteration k.

- Initialization phase: $\mathbf{r}^0 = \mathbf{b} - \mathbf{A}\mathbf{x}^0$ $\mathbf{z}^0 = \tilde{\mathbf{A}}^{-1}\mathbf{r}^0,\ \mathbf{p}^0 = \mathbf{z}^0,\ \mathbf{q}^0 = \mathbf{A}\mathbf{p}^0,\ \eta^0 = \frac{\mathbf{p}^{0^T}\mathbf{r}^0}{\mathbf{p}^{0^T}\mathbf{q}^0}$,
- Repeat for $k = 1, 2...$ until convergence:

Solution estimate		$\mathbf{x}^k = \mathbf{x}^{k-1} + \eta^{k-1}\mathbf{p}^{k-1}$
Residual vector		$\mathbf{r}^k = \mathbf{r}^{k-1} - \eta^{k-1}\mathbf{q}^{k-1}$
Preconditioned residual vector		$\mathbf{z}^k = \tilde{\mathbf{A}}^{-1}\mathbf{r}^k$
Search vector	Using re-orthogonalization	$\mathbf{p}^k = \mathbf{z}^k - \sum_{i=0}^{k-1} \frac{\mathbf{z}^{k^T}\mathbf{q}^i}{\mathbf{p}^{k^T}\mathbf{q}^i}\mathbf{p}^i$
A matrix product vector		$\mathbf{q}^k = \mathbf{A}\mathbf{p}^k$
η estimation	Using re-orthogonalization	$\eta^k = \frac{\mathbf{p}^{k^T}\mathbf{r}^k}{\mathbf{p}^{k^T}\mathbf{q}^k}$

Table I The PCG algorithm

The PCG algorithm equipped with a preconditioner following the rationale of incomplete Cholesky preconditioning features an error matrix $\mathbf{E}_i$. This matrix is dependent on the discarded elements of the lower triangular matrix produced by the incomplete Cholesky factorization procedure. Considering the near-by problems of the form,

$$(\mathbf{K}_0 + \Delta\mathbf{K}_i)\mathbf{u}_i = \mathbf{f}\,, \quad i = 1, ..., n_{sim} \tag{27}$$

If matrix $\mathbf{E}_i$ is taken as $\Delta\mathbf{K}_i$, the preconditioning matrix becomes the initial matrix $\tilde{\mathbf{A}} = \mathbf{K}_0$. The PCG algorithm equipped with the latter preconditioner throughout the entire solution process constitutes the PCG method for the solution of the n_{sim} near-by problems of eq.(27). With the preconditioning matrix $\tilde{\mathbf{A}} = \mathbf{K}_0$ remaining the same during the successive Monte Carlo simulations, the repeated solutions required for the evaluation of the preconditioned residual vector $\mathbf{z}^k = \tilde{\mathbf{A}}^{-1}\mathbf{r}^k$

Prepared using nmeauth.cls DOI: 10.1002/nme

can be treated as problems with multiple right-hand sides, since this vector needs to be evaluated at each PCG iteration k of each simulation i.

5.2. Solution of the augmented SSFEM systems of equations

The augmented systems that are generated when using SSFEM (see eq.(19)) are suitable candidates for iterative solvers since they are flexible enough to be custom tailored to their particular architecture of the augmented systems. A number of solution procedures for solving eq.(19) has been proposed addressing small to medium problems. However, as the problem size grows, such a solution can become quite challenging due to the enormous memory and computational resources required. Solution techniques are based on either Gauss-Jacobi or preconditioned conjugate gradient (PCG) [24, 25] iterative solvers for addressing this problem.

The augmented systems that are generated from the application of SSFEM involve large coefficient matrices that feature a block form. When dealing with Gaussian stochastic fields, each block of the diagonal is comprised of the deterministic stiffness matrix $\mathbf{k}_0$ scaled by an integer. Consider the preconditioning matrix for the case of Gaussian distribution of the form

$$\tilde{\mathbf{A}} = \begin{bmatrix} a_1\mathbf{k}_0 & 0 & \cdots & 0 \\ 0 & a_2\mathbf{k}_0 & \cdots & 0 \\ \vdots & \vdots & \ddots & \vdots \\ 0 & 0 & \cdots & a_n\mathbf{k}_0 \end{bmatrix} \tag{28}$$

where a_n are the coefficients as calculated from the PC basis. For each evaluation of the preconditioned residual vector, the same $\mathbf{k}_0$ matrix needs to be "inverted" n times. This matrix "inversion" is implemented as the solution of n linear systems. Since matrix $\tilde{\mathbf{A}}$ is block diagonal, the solution process can be pipelined as the successive solution of n linear systems with multiple right-hand sides. In lognormal stochastic fields, each block of the diagonal is comprised either of the deterministic stiffness matrix $\mathbf{k}_0$ scaled by an integer or of a linear combination of the deterministic stiffness matrix $\mathbf{k}_0$ and stochastic matrices $\mathbf{k}_1$ to $\mathbf{k}_n$. Matrices $\mathbf{k}_1$ to $\mathbf{k}_n$ may differ up to orders of magnitude when compared to $\mathbf{k}_0$, so the augmented matrix can be considered block-dominant.

Prepared using nmeauth.cls
DOI: 10.1002/nme

6. ADAPTIVE SSFEM BASED ON VRF

As mentioned in the introduction, the aim of the present study is to set up a methodology for building a sparse PC expansion. In this respect, the VRF is used in order to estimate the propagation of the second-order error of the response as a function of the number of terms in the Karhunen-Loève expansion. As a result a spatial adaptation of the number of terms used for describing the random field is achieved in order to obtain a uniform error distribution, leading to a significant reduction of the number of PC coefficients as well as in a significant increase in the sparsity of the corresponding augmented deterministic matrix. The proposed methodology utilizes eq.(25) in order to compute an a priori estimate of the second order error of the response at each degree of freedom of the structure, after estimating the power spectrums which correspond to different number of terms in the KL expansion. This procedure is summarized in the following two distinct phases:

6.1. ***Phase 1: Error estimation***

The first phase consists of the following steps: For each degree of freedom i

(1a) Estimate the variability response function $\text{VRF}_i(\boldsymbol{\kappa})$ numerically, using a fast Monte Carlo simulation as described in the previous section.

(1b) For a target autocorrelation function with corresponding power spectrum $S_f(\boldsymbol{\kappa})$ calculate an "reference" value for the response's variance as

$$\text{Var}^T[U_i] = 2 \cdot \int_0^\infty \text{VRF}_i(\boldsymbol{\kappa}) \cdot S_f(\boldsymbol{\kappa}) d\boldsymbol{\kappa} \tag{29}$$

(1c) Generate realizations of the stochastic field using Karhunen-Loève expansion for various number of terms M and estimate the corresponding power spectrum of the sample function in an ensemble average sense as follows:

$$S_f^M(\boldsymbol{\kappa}) = \frac{1}{2\pi L} \left| \int_0^L f_M(x) e^{-i\boldsymbol{\kappa} x} dx \right|^2 \tag{30}$$

where L is the length of the sample functions of the random fields modeling the uncertainties.

(1d) Calculate the variance of the displacement from:

Prepared using nmeauth.cls DOI: 10.1002/nme

$$\text{Var}^M[U_i] = 2 \cdot \int_0^\infty \text{VRF}_i(\boldsymbol{\kappa}) \cdot S_f^M(\boldsymbol{\kappa}) d\boldsymbol{\kappa} \tag{31}$$

(1e) Estimate the error:

$$\text{Error}^M(U_i) = \frac{\left|\text{Var}^T[U_i] - \text{Var}^M[U_i]\right|}{\text{Var}^T[U_i]} \cdot 100(\%) \tag{32}$$

(1f) Repeat steps $(1c) - (1f)$ with increasing number of terms M until the error of Eq.(32) reaches a target value $(e.g. < 10\%)$ uniformly distributed all over the domain. In general, a different number M_i will be required in each degree of freedom i in order satisfy this criterion.

It must be mentioned here that due to implementation issues, a KL order is assigned to each finite element as the maximum value among the KL orders computed for the corresponding degrees of freedom of this element.

*6.2. **Phase 2: Building a sparse PC coefficient matrix***

The procedure for building the sparse PC coefficient matrix is presented next.

(2a) For each finite element estimate the number of PC terms P_i required for the degree of freedom i according to the formula $P_i = \sum_{k=0}^{p} \binom{M_i+k-1}{k}$.

(2b) The nodal displacement vector is decomposed as $\mathbf{U} = [\mathbf{U}_1, ...\mathbf{U}_j]^T \; j = 1, \ldots, N$ where $\mathbf{U}_j$ are the nodal displacements of N elements. Using the PC expansion the nodal displacements are decomposed as

$$\begin{aligned} \mathbf{U}_1 &= \sum_{i=0}^{P_1} u_i \Psi_i \\ \mathbf{U}_2 &= \sum_{j=0}^{P_2} u_j \Psi_j \\ &\vdots \\ \mathbf{U}_N &= \sum_{k=0}^{P_N} u_k \Psi_k \end{aligned}$$

Prepared using nmeauth.cls
DOI: 10.1002/nme

(2c) Assemble the corresponding sparse PC coefficient matrix and solve the linear system according to eq.(19)

The advantage of the proposed methodology is that the sparsity of the matrix $\mathcal{K}$ in eq.(19) is significantly increased compared to the classical Galerkin approach. The number of PC coefficients that are zero with the proposed methodology depends on the maximum PC basis size and the number of elements with the higher KL order. More specifically, the higher the dispersion of the KL terms in the domain the higher the sparsity increment and, the less the elements with higher KL order in the domain the more the sparsity increase of the augmented matrix.

7. NUMERICAL EXAMPLES

In order to assess the performances of the proposed methodology, a detailed comparison of the classical full PC representation and the proposed sparse one, in terms of by-products of interest, namely the first two statistical moments is performed. Three test examples are considered, one based on a 3D cantilever-type model and two based on a plane stress models. In both cases the elastic modulus is assumed to vary according to the formula,

$$E(\mathbf{x},\theta) = E_0 \cdot \Big(1 + f(\mathbf{x},\theta)\Big) \tag{33}$$

where E_0 is the mean value, $f(\mathbf{x},\theta)$ is assumed to be a one-dimensional, zero-mean homogeneous stochastic field. In the first example $f(\mathbf{x},\theta)$ is assumed one-dimensional and Gaussian, while in the second and third example it follows a lognormal distribution, which varies spatially in both directions. We must state here that in the first example where a Gaussian random field was used, in order to avoid phenomena with negative values for the Young's modulus, a small value was selected for the standard deviation ($\sigma = 0.1$). The mean values μ and standard deviations σ are reported in Table 2, while the autocorrelation function is given by the following equations for one- and two-dimensional random fields, respectively:

$$R_f(\tau) = \sigma^2 e^{-\frac{|\tau|}{b}}, \qquad R_f(\tau_1,\tau_2) = \sigma^2 e^{-(\frac{|\tau_1|}{b_1} - \frac{|\tau_2|}{b_2})} \tag{34}$$

where κ is the wave number and b the correlation length parameter. Their corresponding power

Prepared using nmeauth.cls
DOI: 10.1002/nme

spectrums can be obtained using the Fourier transform.

Test Case	**Distribution**	E_0 (KN/m^2)	σ
Cantilever	$\mathcal{N}(\mu, \sigma^2)$	2.1×10^7	0.1
2D rectangular plate	ln$\mathcal{N}(\mu, \sigma)$	1.0×10^6	0.6
2D L-shaped plate	ln$\mathcal{N}(\mu, \sigma)$	2.1×10^7	0.6

Table II Test cases - input random variable

7.1. 3D model of a Cantilever structure

Consider the 3D model of a cantilever structure of Fig.1 with length $L = 10\ m$ and section $A = 0.25 \times 0.5\ m^2$, loaded with a deterministic load $p = 10\ KN/m^2$, uniformly distributed in the nodes of the top edge of the cantilever. The nodes of the starting section of the cantilever are fixed against translations. The cantilever is discretized with 402 HEXA finite elements resulting in a problem with $n_{dof} = 5412$. The value $b = 5\ m$ is selected for the correlation length parameter of eq.(34) for this example.

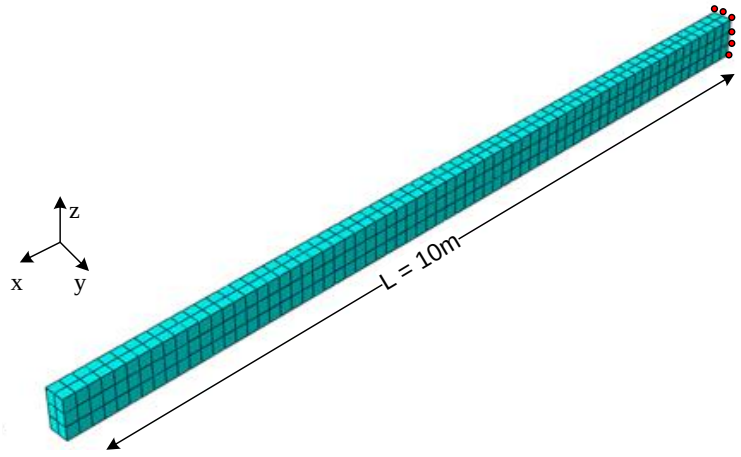

Figure 1 Finite element mesh and boundary conditions of 3D-cantilever model

Figure 2 presents the plots of the power spectrums S_f^M for various values of M together with the target power spectrum (eq.(34)), all computed via the Fourier transform of the autocorrelation function of eq.(30). From this Fig. it can be seen that as M increases, S_f^M converges gradually to

Prepared using nmeauth.cls
DOI: 10.1002/nme

the target power spectrum. At S_f^8, the 95% of the total area is covered. Figure 3 presents plots of the VRF calculated at locations $x_1 = 2.5\ m$, $x_2 = 7\ m$ and $x_3 = 10\ m$ together with the plot of S_f^8. The $\text{VRF}_i(\kappa)$ is estimated numerically along the $x-$axis of the cantilever, in the range $\kappa \in [0, \kappa_u]$, κ_u being an upper cut-off frequency, taken equal to 4 rad/m.

Inspection of Fig.3, keeping in mind that the variance is given by the integral form expression of eq.(25), reveals that the error of the variance depends not only on the number M but also on the values of the VRF at the frequencies that are not well represented in the power spectrum due to the KL truncation. Thus, the error for $x_1 = 2.5\ m$ and $M = 8$ is expected to be smaller than the same error for $x_2 = 7\ m$ and the error at $x_2 = 7\ m$ is smaller than the one at $x_3 = 10\ m$ since, at the latest location the VRF has significant contributions at frequencies larger than the frequency at which S_f^8 becomes zero ($\kappa_u^5 = 0.5$), while for $x_1 = 2.5\ m$ and $\kappa > 0.5$, VRF becomes almost zero. Indeed, the corresponding errors computed via eq.(32) are found to be 6%, 14% and 17.5% respectively. This error behavior is presented concisely in Fig.4, which plots the $(\%)$ error computed via eq.(32) for the three representative locations $x_1,\ x_2$ and x_3 as a function of M. As we can see, the error is much smaller for $x_1 = 2.5\ m$ and small number of M for the reasons previously mentioned. Figure 5 depicts the areas with values up to a certain M required to reach a target error less than a fixed value. More specifically, if we require a uniform error less than 15% then for all the points in Area I the values $1 \leq M_I \leq 5$ are required, for points inside Area II we need $5 \leq M_{II} \leq 7$, while for all the other points in Area III, $7 \leq M_I \leq 9$ is satisfying the requirement. Thus, we choose to represent all stochastic degrees of freedom in Area I with $M = 2$, in Area II with $M = 6$ and $M = 8$ for Area III.

Prepared using nmeauth.cls
DOI: 10.1002/nme

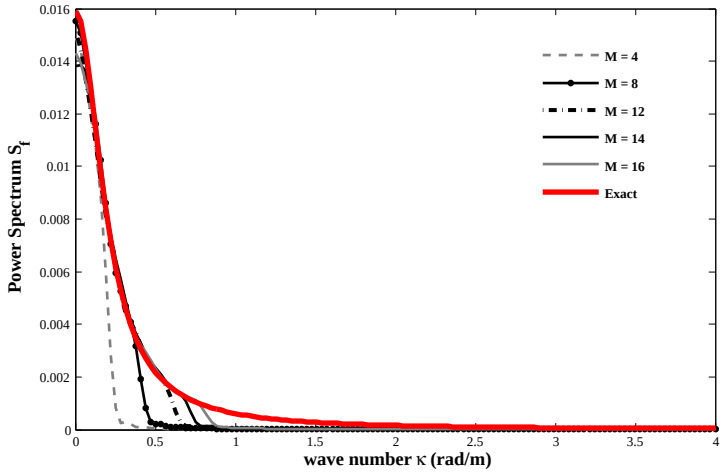

Figure 2 Calculated power spectrums for various values of KL order M together with the exact power spectrum

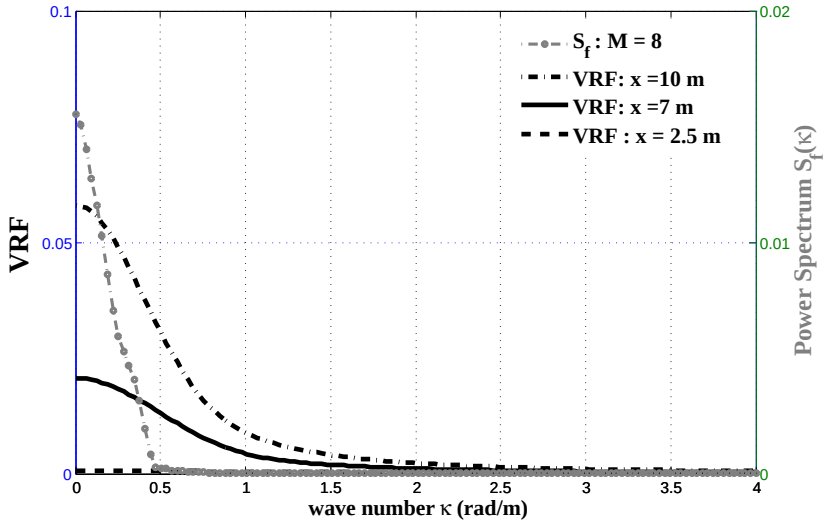

Figure 3 Joint plot of S^8_{ff} with VRF($x_1 = 2.5\ m$), VRF($x_2 = 7\ m$), VRF($x_3 = 10\ m$)

Prepared using nmeauth.cls
DOI: 10.1002/nme

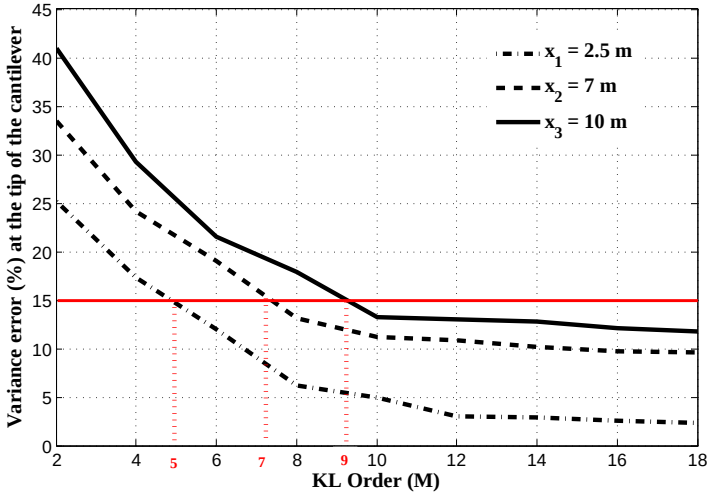

Figure 4 Variance error (%) as a function of M

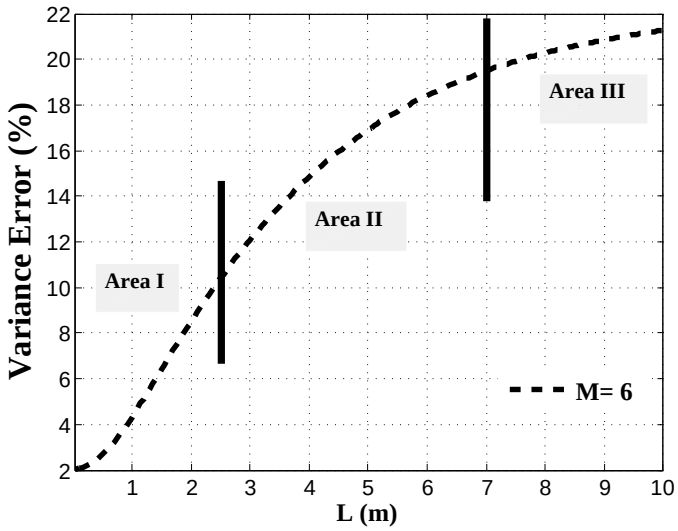

Figure 5 Subdomains with the same number of M

This problem is first solved with the classical PC expansion method with M = 2, 6 and 8 all over the domain and p = 2, 3 and 4. The z-axis displacement U_z at the tip ($x_3 = 10\ m$) and its standard deviation σ_z, are monitored in order to obtain the results, which are presented in Table 3. From this Table it can be seen that the minimum error computed with eq.(32) is achieved for M=8 and p=4 as expected and it is 11.17 %.

Prepared using nmeauth.cls
DOI: 10.1002/nme

$(\boldsymbol{M}, \boldsymbol{p})$	U_z (m)	σ_z (m)	$\boldsymbol{Error}^{(M)}(\%)$
(2,2)	-0.2265	0.0172	42.15
(6,2)	-0.2275	0.0197	26.23
(8,2)	-0.2284	0.0202	12.95
(2,3)	-0.2280	0.0195	38.22
(6,3)	-0.2281	0.0206	23.15
(8,3)	-0.2285	0.0214	11.99
(2,4)	-0.2283	0.0201	39.12
(6,4)	-0.2285	0.0209	22.81
(8,4)	-0.2285	0.0222	11.17

Table III Standard PC expansion

The same calculation is repeated using the proposed adaptive sparse PC methodology described in section 5. For this calculation the different values of M = 2, 6 and 8 are used for areas (I), (II) and (III) respectively (see Fig.5). The corresponding results for p = 2, 3 and 4 are presented in Table 4 together with the $(\%)$ relative error, with respect to the classical PC. This Table also depicts the $(\%)$ sparsity increase of the PC coefficient matrix for each case. From these results it can be seen that the same level of accuracy is achieved in all cases with the one of the classical PC using $M = 8$ everywhere. However, this accuracy is reached with a 40% sparsity increase of the coefficient matrix.

$(\langle M_I, M_{II}, M_{III}\rangle, p)$	U_z (m)	σ_z (m)	Error $(\%)$	**Sparsity**$(\%)$
$(\langle 2, 6, 8\rangle, 2)$	-0.2284	0.0197	4.06	+38.63
$(\langle 2, 6, 8\rangle, 3)$	-0.2285	0.0212	1.39	+41.17
$(\langle 2, 6, 8\rangle, 4)$	-0.2285	0.0221	0.45	+43.21

Table IV Adaptive PC expansion

A visual representation of the sparsity increase for this problem is presented in Fig.6.

Prepared using nmeauth.cls
DOI: 10.1002/nme

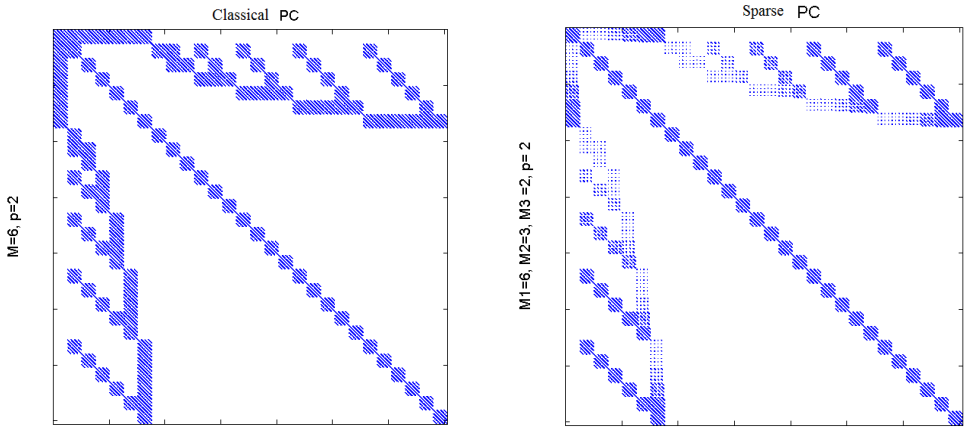

(a) (b)

Figure 6 Non-zero elements of the : (a) full PC and (b) sparse PC

7.2. Plane stress with 2D lognormal random field

Next, the case of a 2D lognormal random field is investigated in order to show the performance of the method in a non-Gaussian case. The two-dimensional domain of Fig.7 is a rectangle of length $L_x = 1\ m$, width $L_y = 1\ m$ and thickness equal to one. The domain is divided with a uniform mesh of 20×20 quadrilateral plane stress finite elements. The model is subjected to a constant deterministic uniform load $p = 100\ KN/m$ along its boundary at its upper side. The Young's modulus E is considered to vary randomly in both directions, following a lognormal distribution $\ln\mathcal{N}(\mu, \sigma)$ with mean value $\mu = 0$ and σ equal to 0.6. The correlation length parameters are selected arbitrary for this case to be $b_1 = b_2 = 1\ m$. A schematic view of the corresponding power spectrum of the underlying Gaussian field is given in Fig.8. The VRF for this example is estimated with FMCS technique according to eq.(23). The number of MCS per wave number dyad (κ_x, κ_y) required is usually 5-10, the cost of which must be added to the total computational cost of the procedure. Indicative plots of the VRFs, at point x_1, x_2 and x_3 are shown in Figs.9 to 11, respectively.

After estimating the variability response function in each degree of freedom, we calculate the power spectrum of the lognormal field S_l^M. The variance of the vertical displacement in each location of the plate is then calculated using the analytic expression of eq.(25) and thus the error for

Prepared using nmeauth.cls DOI: 10.1002/nme

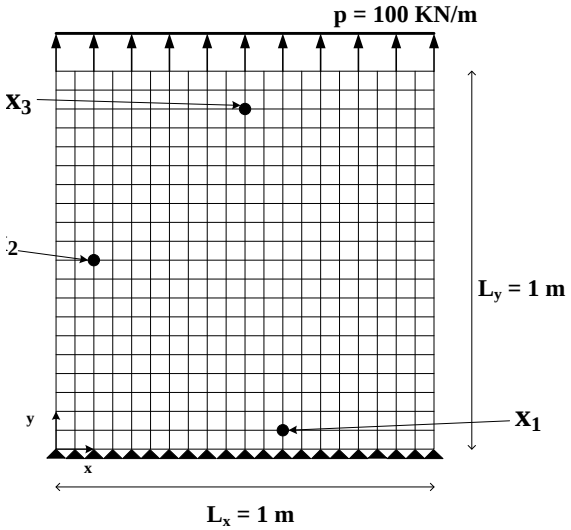

Figure 7 Two-dimensional plate

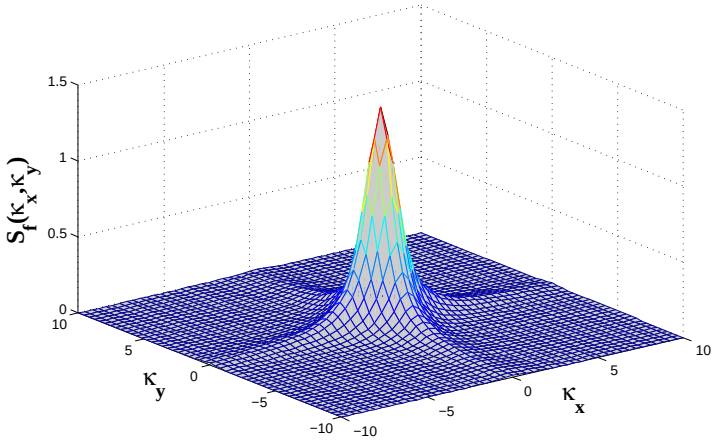

Figure 8 Spectral density function of the underlying Gaussian random field

all locations of the domain as a function of M is derived. This error behavior is presented concisely in Fig.12, which plots the $(\%)$ error for the three representative locations shown in Fig.7 ($x_1,\ x_2$ and x_3) as a function of M. It must be mentioned that this variance error is computed with respect to the target variance obtained for $M = 10$ in the KL terms. From this figure it can be seen that the values M=2,3 and 6 are required for points $x_1,\ x_2$ and x_3, respectively, in order to reach the same error level (2.5%). Figure 13 depicts the distribution of the KL order along the domain required to reach a target error of about 2.5%. More specifically, for the all the finite elements of subdomain

Prepared using nmeauth.cls
DOI: 10.1002/nme

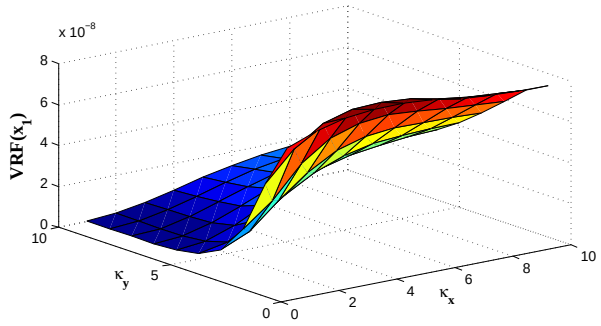

Figure 9 Computed **VRF** at location x_3

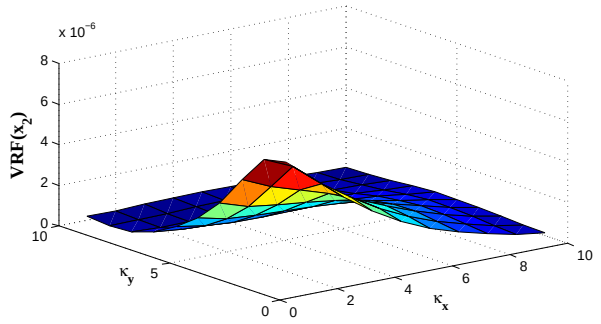

Figure 10 Computed **VRF** at location x_2

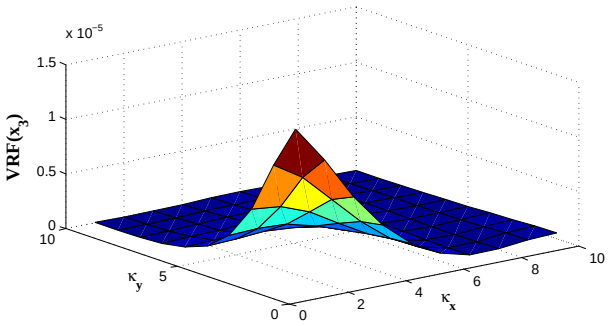

Figure 11 Computed **VRF** at location x_3

(I) the value of up to M_I = 2 is required, for finite elements of subdomain (II) we need M_{II}=3, while for all the other finite elements of subdomain (III), M_{III}=6 is satisfying the requirement for a uniform error.

Prepared using nmeauth.cls
DOI: 10.1002/nme

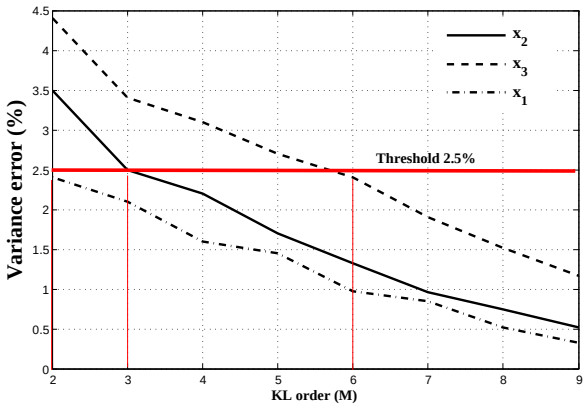

Figure 12 Variance error (%) as a function of M in three representative locations x_1, x_2 and x_3

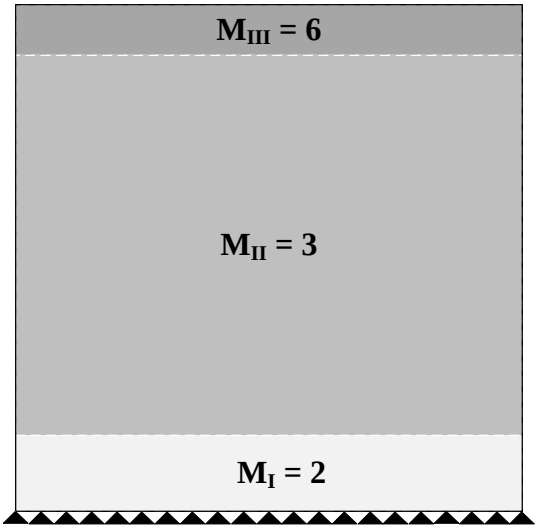

Figure 13 Subdomains with equal M values required to reach a target error of about 2.5%

This problem is initially solved with the classical PC expansion method for M = 2, 3 all over the domain and 6 and p = 2, 3 and 4. The y-axis displacement (U_y) of the upper node of the plate, is monitored in order to obtain the results, which are presented in Table 5. The same calculation is repeated using the proposed adaptive sparse PC methodology. For this calculation the different values of M = 2, 3 and 6 are used (see Fig.13)and the corresponding results for p = 2, 3 and 4 are presented in Table 6. Figures 14 and 15 depict the relative error in the mean and standard deviation

DOI: 10.1002/nme

M	**p**	$\mathbf{U}_y$ $(\times 10^{-3})$ (m)	σ_y $(\times 10^{-4})$
2	2	2.2	3.785
3		2.17	3.882
6		2.36	3.992
2	3	2.29	3.796
3		2.23	3.89
6		2.39	4.002
2	4	2.25	3.80
3		2.29	3.894
4		2.401	4.00

Table V Standard PC expansion

$(\mathbf{M}_I, \mathbf{M}_{II}, \mathbf{M}_{III})$	**p**	$\mathbf{U}_y$ $(\times 10^{-3})$ (m)	σ_y $(\times 10^{-4})$
(2,3,6)	2	2.2985	3.803
	3	2.3114	3.877
	4	2.412	3.988

Table VI Sparse PC expansion

of U_y, as a function of p for both approaches, respectively. These errors of the classical PC with $M = 2$ and $M = 3$ and the sparse PC expansion, are computed with respect to the classical PC with $M = 6$, which is considered a reference solution for all cases. It must be highlighted that, as shown in Figs.14 and 15, this error is less than 1% for the sparse PC. Figures 16 and 17 depict the sparsity of the augmented matrix for the plane stress problem of section 7.2, as a function of p. From these figures we can see that, depending on the value of p, a sparsity increase of order $40 - 70\%$ can be reached, when the sparse PC method is implemented with $M = 2$, $M = 3$ and $M = 6$. The non-zero elements of the augmented matrix are almost one order of magnitude less with the proposed methodology compared to the classic PC with $M = 6$ all over the domain. Finally, plots of the non-zero elements of the augmented matrix is shown in Fig.18 for the full PC with $M = 6$ and $p = 3$ and for the sparse PC approach with $M_I = 3,\ M_{II} = 2\ M_{III} = 6$ and $p = 3$, respectively.

Prepared using nmeauth.cls DOI: 10.1002/nme

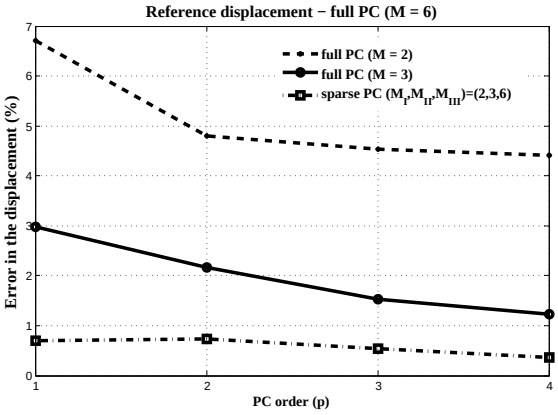

Figure 14 Relative error $(\%)$ of the mean displacement U_y as a function of p

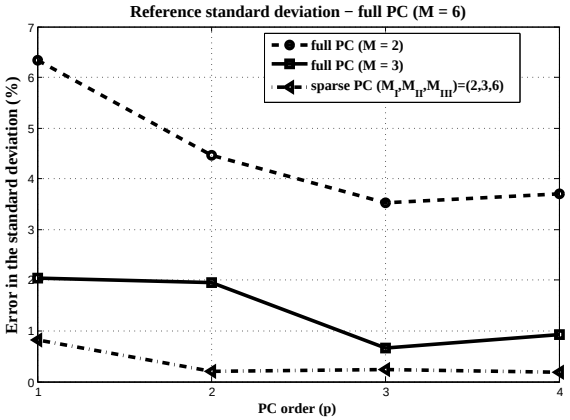

Figure 15 Relative error $(\%)$ of the standard deviation σ_y of U_y as a function of p

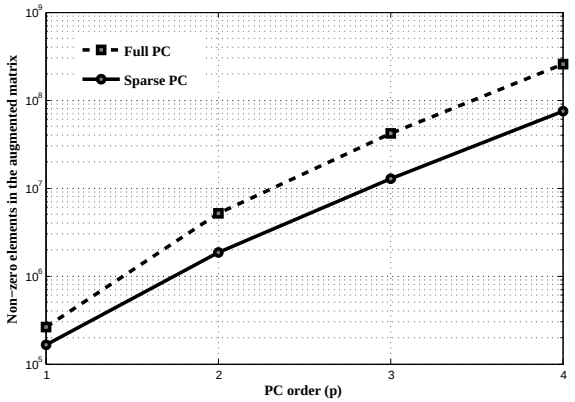

Figure 16 Sparsity of the augmented matrix -sparse PC vs full PC ($M = 6$)

Prepared using nmeauth.cls
DOI: 10.1002/nme

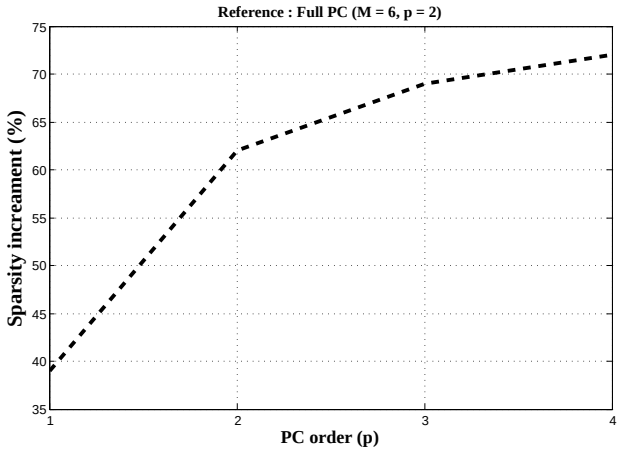

Figure 17 Increase of sparsity of the augmented matrix as a function of p

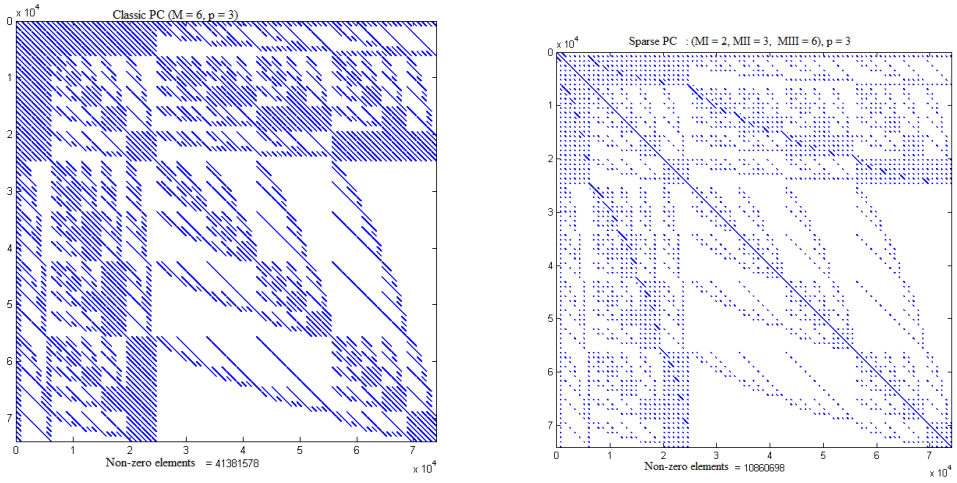

(a) (b)

Figure 18 Non-zero elements of the : (a) full PC and (b) sparse PC

7.3. L-shape, 2D plane stress problem

As a final numerical example, the proposed methodology is applied in a 2D, L-shaped domain problem under static loading. This example aims in demonstrating the applicability of the method in a more complex example in which the spatial variation of the VRF and thus the corresponding KL order are expected to be significant. The geometric properties of the domain are shown in Fig.19

Prepared using nmeauth.cls DOI: 10.1002/nme

along with its boundary conditions and the applied loads. The finite element mesh consists of 619 three-node plane stress triangular elements with a total of $n_{dof} = 682$.

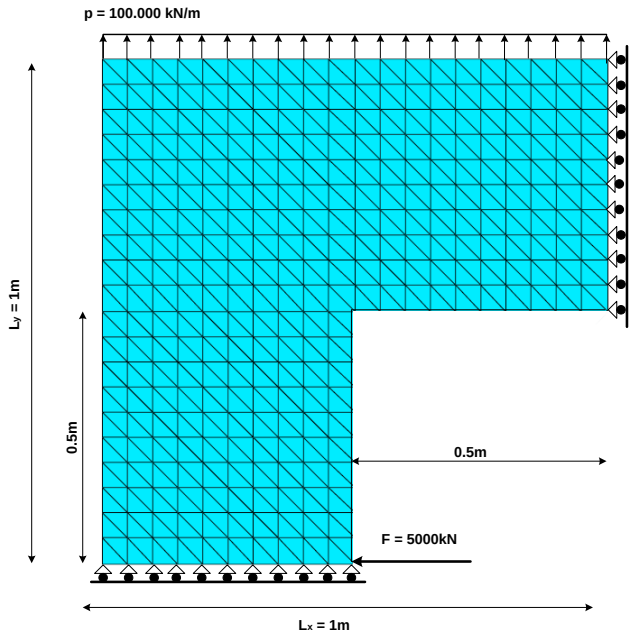

Figure 19 L-shaped domain under static loading

Again, the Young's modulus E is described by a two-dimensional lognormal random field with the characteristics as described in section 7.2. Steps (1a) to (1f) of Phase 1 of the proposed methodology are first implemented in order to estimate the spatial distribution of the KL truncation order M. The final spatial distribution of the KL terms is constructed from the maximum order M of each degree of freedom. In Figs. 20(a) and (b) we see the spatial distributions of the KL terms obtained for x- and y- displacement, respectively while Fig.21 depicts the final KL order spatial distribution. As we can see from Fig.20(a) the distribution of the KL orders obtained from the x-displacement is uniform all over the domain, equal to $M = 3$, except in two areas, one in the upper left corner and on the bottom of the domain where the required KL order is increased and reaches a value of $M = 4$. For the case of the y-displacement of Fig.20(b) the dispersion in the spatial KL distribution is more pronounced where we see that the value of $M = 3$ is limited in a short stripe at

Prepared using nmeauth.cls
DOI: 10.1002/nme

the left side of the domain and in the inner side of the L-shape while the value $M = 4$ is dominant at the right edge of the domain and in a vertical stripe. Finally, there exist a small area where a value of $M = 5$ is required in order to satisfy the uniform criterion of the error at the bottom of the L-shaped domain. The final KL order distribution (see Fig.21) is a combination of these distributions with the maximum value of M to be assigned in each element.

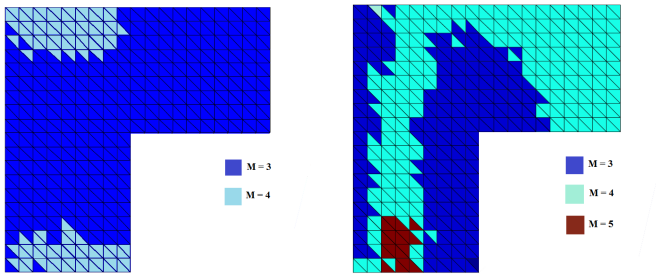

(a) (b)

Figure 20 KL order spatial distribution at the degrees of freedom of a) x-directions b) y-direction

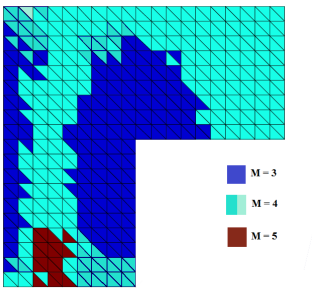

Figure 21 Final KL order distribution of the domain

After having estimated the spatial distribution of the KL order in the domain we proceed in ***Phase 2*** where we construct the sparse PC basis as described in section 6 and we estimate the mean value of the displacement field and its corresponding variance. The mean value of the x- and y- displacements are contoured in Fig.22(a) and (b). As it is expected, the variation of the mean x-displacements is horizontally; the minimum displacements appear in the top of the domain and their values increase towards the bottom side reaching a maximum value of $0.06m$ at the bottom right corner. For the mean y-displacements we see that their values change along the vertical axis; their values increase

Prepared using nmeauth.cls
DOI: 10.1002/nme

from the left to the right reaching a maximum value of $0.08m$ at the right edge of the structure. The variance of the mean x- and y- displacements are contoured in Fig.23(a) and (b), respectively. As we can see from these Figs. a similar to the displacements behavior, regarding their distribution along the structure, is observed to the variances. More specifically, the variance of the horizontal displacements is practical zero at the top edge of the structure and its values are increasing as we move towards the bottom side, reaching a high value of 8×10^{-4}, while the variance of the vertical displacements is increasing from the left to the right with a maximum value of 17×10^{-4} at the upper right corner.

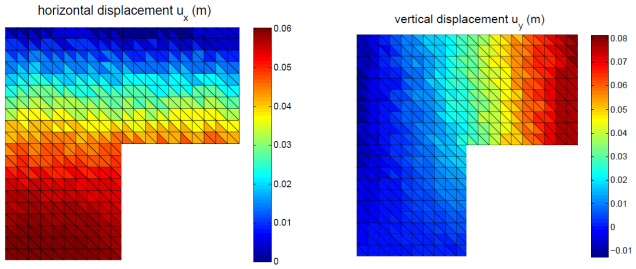

(a) (b)

Figure 22 Mean value of the a) x-displacement field b) y-displacement field, estimated with the adaptive SSFEM for $p = 4$

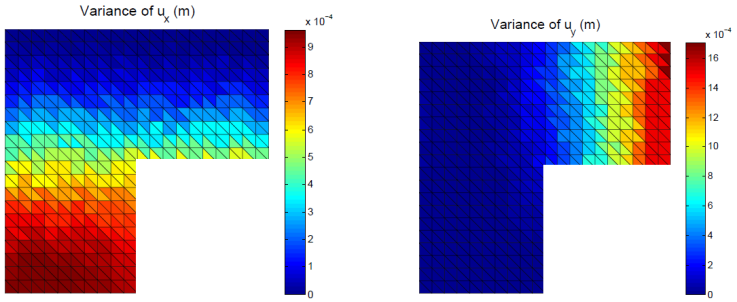

(a) (b)

Figure 23 Variance of the a) x-displacement field b) y-displacement field, estimated with the adaptive SSFEM for $p = 4$

Prepared using nmeauth.cls
DOI: 10.1002/nme

Finally, Fig.24 shows the mean squared error in the estimation of the mean value and its corresponding variance of the displacement field with the proposed methodology and with the standard SSFEM method with $M = 5$ uniformly all over the domain for $p = 3, 4$ and 5. We see that this error is less than 0.1% for the mean displacement field in all cases while for its variance reduces from 4% for $p = 3$ to less than 1% for $p = 5$, in both directions.

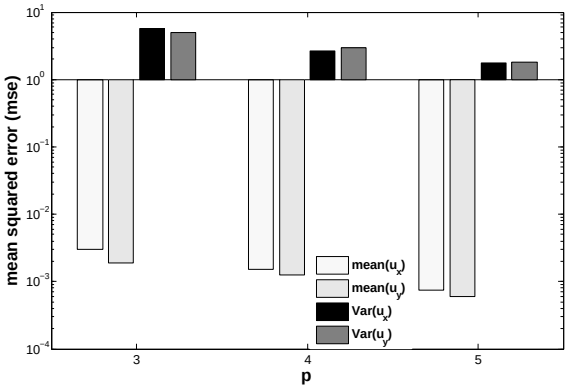

Figure 24 Total mean squared error (mse) of the mean and variance of the displacement field estimated with the proposed methodology and with the standard SSFEM with $M = 5$ all over the domain and $p = 3$, 4 and 5

8. COMPUTATIONAL PERFORMANCE OF THE PROPOSED METHOD

The enhancement of the computational performance of the proposed approach due to the aforementioned increase in the sparsity of the coefficient matrix is demonstrated in Table 7. The computational platform used is an Intel Core i7 X980 with 6 physical cores at 3.33 GHz with 24 GB of RAM while the actual implementation was serial, using only one of the six available cores. In order to assess the computational cost of the proposed approach, the cost required for the calculation of the VRF must also be considered. Since this calculation is used in order to obtain an a priori rough error estimation, the VRF can be computed with a relatively sparse discretization in the frequency domain. Therefore, a value of $N = 5$ in eq.(23) is expected to be sufficient for the purposes of this

Prepared using nmeauth.cls
DOI: 10.1002/nme

estimation, leading to an additional cost of 50-100 MCS, which of course should be added to the cost of the adaptive sparse PC solution. In order to minimize the cost of these MCS, the PCG method described in section 5.1 is utilized.

In this Table it can be seen that for the example of section 7.2 a 75% reduction of the total computing time was achieved with the sparse SSFEM approach compared to the full SSFEM method, even with the addition of the extra 100 MCS required for the calculation of the VRF which takes 1% of the total computation time. The sparse SSFEM solution was achieved with 32 PCG iterations instead of 40 required for the full problem. In the example of section 7.3 the reduction of the computational time was much higher with respect to the previous example reaching an almost two orders of magnitude improvement of the computational efficiency. The sparse SSFEM solution was achieved with 52 PCG iterations instead of 330 required for the full problem. This is attributed to the increased size of the coefficient matrix of the last example due to the implementation of a higher order polynomial chaos $p = 5$ instead of $p = 3$. Thus, the gaining from using the proposed approach is more significant in large systems, requiring high order of PC approximations.

			SSFEM			
			Example 2		**Example 3**	
	Factorization	**Direct solution** (1 MCS)	**Full** (40 iter.)	**Sparse** (32 iter. + 100 MCS)	**Full** (330 iter.)	**Sparse** (52 iter. + 100 MCS)
Computing time (sec)	0.021	0.0004871	23.437	6.06279+0.06971	640.23	15.12+0.06971

Table VII Computational performance of classical SSFEM (Full problem) vs adaptive SSFEM (Sparse problem)

9. CONCLUSIONS

In this paper a methodology is described to construct an adaptive sparse polynomial chaos (PC) expansion of the response of stochastic systems whose input parameters are independent random variables modeled as random fields. The proposed methodology utilizes the concept of variability response function (VRF) in order to compute an a priori inexpensive estimate of the spatial distribution of the second-order error of the response as a function of the number of terms used

Prepared using nmeauth.cls
DOI: 10.1002/nme

in the truncated KL series representation of the random fields involved in the problem. As a result a spatial adaptation of the number of terms used for describing the random field is achieved in order to obtain a uniform error distribution, leading to a significant reduction of the number of PC coefficients and a corresponding increase in the sparsity of the augmented deterministic matrix. This sparsity increase improves significantly the computational performance of the SSFEM. The benefits of using the proposed adaptive procedure are more pronounced in large FE stochastic systems which require high orders of PC approximations. The extension of the proposed method to nonlinear cases is considered for future work.

ACKNOWLEDGEMENTS

This work has been supported by the European Research Council Advanced Grant MASTER - Mastering the computational challenges in numerical modeling and optimum design of CNT reinforced composites ($ERC - 2011 - ADG - 20110209$).

REFERENCES

1. Stefanou G. The stochastic finite element method: Past, present and future. *Computer Methods in Applied Mechanics and Engineering* 2009; **198**:1031–1051.
2. Ghanem R, Spanos P. *Stochastic finite elements - A spectral approach*. 1991.
3. Loeve M. *Probability Theory*. 1977.
4. Rahman A S. A polynomial dimensional decomposition for stochastic computing. *International Journal for Numerical Methods in Engineering* 2008; **76**:2091–2116.
5. Rahman A S. Extended polynomial dimensional decomposition for arbitrary probability distributions. *Journal of Engineering Mechanics* 2009; **135(12)**:1439–1451.
6. Rahman A S, Yadav V. Orthogonal polynomial expansions for solving random eigenvalue problems. *International Journal for Uncertainty Quantification* 2011; **1(2)**:163–187.
7. Rahman A S. A generalized anova dimensional decomposition for dependent probability measures. *SIAM/ASA Journal on Uncertainty Quantification* 2014; **2**:670–697.
8. Blatman G, Sudret B. An adaptive algorithm to build up sparse polynomial chaos expansions for stochastic finite element analysis. *Probabilistic Engineering Mechanics* 2010; **25(2)**:183–197.

Prepared using nmeauth.cls
DOI: 10.1002/nme

9. Blatman G, Sudret B. Adaptive sparse polynomial chaos expansion based on least angle regression. *Journal of Computational Physics.* 2011; **230(6)**:2345–2367.
10. Adhikari S. A reduced spectral function approach for the stochastic finite element analysis. *Computer Methods in Applied Mechanics and Engineering* 2011; **200(21–22)**:1804–1821.
11. Ghosh D, Avery P, Farhat C. A method to solve spectral stochastic finite element problems for large-scale systems. *International Journal Numerical Methods Engineering* 2008; **00**:1–6.
12. Panayirci H. Efficient solution of Galerkin-based polynomial chaos expansion systems. *Advanced Engineering Software* 2010; **41**:1277–1286.
13. Yadav V, Rahman A S. Adaptive-sparse polynomial dimensional decomposition for high-dimensional stochastic computing. *Computer Methods in Applied Mechanics and Engineering* 2014; **274**:56–83.
14. Shinozuka M. Structural response variability. *Journal Engineering Mechanics, (ASCE)* 1987; **113**:825–842.
15. Teferra K, Deodatis G. Variability response functions for beams with nonlinear constitutive laws. *Probabilistic Engineering Mechanics* 2012; **29**:139–148.
16. Papadopoulos V, Deodatis G. Response variability of stochastic frame structures using evolutionary field theory. *Computer Methods in Applied Mechanics and Engineering* 2006; **195 (9-12)**:1050–1074.
17. Papadopoulos V, Deodatis G, Papadrakakis M. Flexibility-based upper bounds on the response variability of simple beams. *Computer Methods in Applied Mechanics and Engineering* 2005; **194 (12-16)**:1385–1404.
18. Wall F, Deodatis G. Variability response functions of stochastic plane stress/strain problems. *Journal of Engineering Mechanics* 1994; **120 (9)**:1963–1982.
19. Arwade S, Deodatis G. Variability response functions for effective material properties. *Probabilistic Engineering Mechanics* 2010; **26**:174–181.
20. Deodatis G, Graham L, Micaletti R. A hierarchy of upper bounds on the response of stochastic systems with large variation of their properties: random variable case. *Probabilistic Engineering Mechanics* 2003; **18 (4)**:349–364.
21. Miranda M, Deodatis G. On the response variability of beams with large stochastic variations of system parameters. 2006.
22. Papadopoulos V, Papadrakakis M, Deodatis G. Analysis of mean response and response variability of stochastic finite element systems. *Computer Methods in Applied Mechanics and Engineering* 2006; **195 (41-43)**:5454–5471.
23. Deodatis G, Miranda M. Generalized Variability Response Functions for Beam Structures with Stochastic Parameters. *Journal Engineering Mechanics* 2012; **1**:340.
24. Ghanem R, Kruger R. Numerical solution of spectral stochastic finite element systems. *Computer Methods in Applied Mechanics and Engineering* 1996; **129**:289–303.
25. Pellissetti M, Ghanem R. Iterative solution of systems of linear equations arising in the context of stochastic finite elements. *Advanced Engineering Software* 2000; **31**:607–616.
26. Grigoriu M. Evaluation of Karhunen-Loève, spectral and sampling representations for stochastic processes. *Journal of Engineering Mechanics* 2006; **132**:179–189.

Prepared using nmeauth.cls
DOI: 10.1002/nme

27. Huang S, Quek S, Phoon K. Convergence study of the truncated Karhunen-Loève expansion for simulation of stochastic processes. *International Journal of Numerical Methods in Engineering* 2001; **52**:1029–1043.
28. M G. Applied non-Gaussian processes. *New Jersey: Prentice Hall* 1995; .
29. M G. Crossings of non-Gaussian translation processes. *Journal of Engineering Mechanics* 1984; **110**:610–620.
30. Sakamoto S, Ghanem R. Simulation of multi-dimensional non-Gaussian non-stationary random fields. *Probabilistic Engineering Mechanics* 2002; **17**:167–176.
31. Sakamoto S, Ghanem R. Polynomial chaos decomposition for the simulation of non-Gaussian nonstationary stochastic processes. *Journal of Engineering Mechanics* 2002; **128**:190–201.
32. Ghanem R. The nonlinear Gaussian spectrum of log-normal stochastic processes and variables. *Journal Applied Mechanics* 1999b; **66**:964–973.
33. Sudret B, der Kiureghian A. Stochastic finite element methods and reliability: a state-of-the-art report. *Rep. No. UCB/SEMM-2000/08, University of California at Berkeley, USA* 2000; **24**:619–644.
34. R C, Martin W. The orthogonal development of nonlinear functionals in series of Fourier-Hermite functionals. *Ann. of Math.* 1947; **48(2)**:385–392.
35. Lucor D D Xiu, Karniadakis G. Spectral representations of uncertainty in simulations: Algorithms and applications. *In Proceedings of the International Conference on Spectral and High Order Methods (ICOSAHOM-01), Uppsala, Sweden* 2001; .
36. Papadrakakis M, Papadopoulos V. Robust and efficient methods for stochastic finite element analysis using Monte Carlo simulation. *Computer Methods in Applied Mechanics and Engineering* 1996; **134**:325–340.
37. Papadrakakis M, Kotsopoulos A. Parallel solution methods for stochastic finite element analysis using Monte Carlo simulation. *Computer Methods in Applied Mechanics and Engineering* 1999; **168**:305–320.
38. Charmpis D, Papadrakakis M. Improving the computational efficiency in finite element analysis of shells with uncertain properties. *Computer Methods in Applied Mechanics and Engineering* 2005; **194**:1447–1478.

Prepared using nmeauth.cls
DOI: 10.1002/nme